journal

J. Am. Ceram. Soc., 95 [3] 1128–1137 (2012)
DOI: 10.1111/j.1551-2916.2011.05058.x

Evidence on the Dual Nature of Aluminum in the Calcium-Silicate-Hydrates Based on Atomistic Simulations

Mohammad Javad Abdolhosseini Qomi,[‡,†] Franz-Josef Ulm,[‡] and Roland J.-M. Pellenq[‡,§]

[‡]Department of Civil and Environmental Engineering, Massachusetts Institute of Technology, Cambridge, MA

[§]Centre Interdisciplinaire des Nanosciences de Marseille, Centre National de la Recherche Scientifique and Marseille Université′, Marseille, France

Hydration of tri-calcium silicate (C_3S) and di-calcium silicate (C_2S) precipitates calcium-silicate-hydrate (CSH) which is the bonding phase responsible for the strength of cementitious materials. Substitution of part of C_3S and C_2S with aluminum-containing additives alters the chemical composition of hydration products by precipitating calcium-aluminate-silicate-hydrate (CASH). Incorporation of aluminum in the molecular building blocks of CSH entails structural and chemo-mechanical consequences. These alterations can be measured through solid state nuclear magnetic resonance (NMR) experiments. By conducting a wide spectrum of atomistic simulation methods on thousands of aluminum-containing molecular CASH structures, an overall molecular approach for determination of CASH nanostructure is presented. Through detailed analysis of different order parameters, it is found that aluminum can exhibit a tetra-/penta-/octahedral behavior which is fully consistent with the recent NMR observations. This corresponds to the formation of a class of complex three-dimensional alumino-silicate skeletons with partial healing effect in the CASH nanostructure potentially increasing durability and strength of hydration products. We explored the variation of mechanical observables by increasing aluminum content in CASH structures of varying calcium to silicon ratio. Finally, deformation of CSHs and CASHs of different chemical formula in a multi-scale fashion unravels the effect of chemical composition on the strength and kinematics of deformation in this particular type of composites.

I. Introduction

CALCIUM-ALUMINATE-SILICATE-HYDRATE (CASH) is the major hydration product of calcio-silicate systems mixed with reactive aluminum-enriched materials. Although minor traces of aluminum can be present as guest ions in clinker phases such as alite (C_3S) and belite (C_2S),[1] calcium aluminate (C_3A), ferrite (C_4AF),[2] certain class of fly ashes and slags have substantial amount of aluminum. Intrinsically, hydration of such a complex system results in a multifarious texture ranging from nano-scale particles[3] to porous inhomogeneous micrometer-scale texture with interesting binding property and structural strength.[4] So far, at the bottom of the length spectrum, the molecular representation of CASH nano-structure has been elucidated by analogy based on the structure of aluminum-containing tobermorite minerals.[5–8] Tobermorites are a class of low calcium to silicon ratio (C/S $\leq$ 1) calcium-silicate-hydrates (CSH), composed of pseudo-octahedrally coordinated calcium sheets sandwiched by infinite and parallel silica chains on both sides. Interlayer spacing is filled with calcium and water molecules; the amount of extra calcium ions hence the C/S ratio being related to the electrical charge on the calcium oxide sheets needed to maintain electro-neutrality. However, in a conventional cement paste with average C/S ratio of 1.7,[9] the tetrahedral silica chains mostly consist of dimmers with a few monomers and pentamers.[10–13] These defective silica chains lead to an overall disordered glassy nanotexture away from the conventional picture based on crystalline tobermorite or Jennite (another CSH mineral). In the present work, we aim at providing CASH nanotexture in a similar way as for the aluminum-free cCSH model of cement presented in.[13]

Nuclear magnetic resonance (NMR) experiment has shown that the nanostructure of CASH nano-composites strongly depends on C/S ratio.[14–16] It is stated (i) that aluminum substitutions occur in tetrahedrally coordinated silica sites for low C/S ratios whereas (ii) it occurs in octahedrally coordinated sites for high C/S gels. In low C/S regimes, the tetrahedral aluminum is most probably due to tetrahedral substitution in the silica chains of CSH.[17–20] For high C/S ratio gels (which correspond to real cement), the position of aluminum has been unknown and was attributed to the substitution in the interlayer spacing,[21–23] on the particle surfaces[23] or other hydration products.[24] The latter type of aluminum is mostly octahedral with traces of pentahedral coordination.[25] The ratio of aluminum atoms with octahedral coordination to aluminum atoms with pentahedral coordination is about 3.5.[23] In this context, the increase in the mean chain length[16,17] and the formation of interlayer silica connections[26] cannot be consistently explained by aluminum being a simple silicon to aluminum substitutions. In addition, the recent state of the art ^{29}Si & ^{27}Al NMR study (coupled with ^{1}H NMR) published by Rawal *et al.*[23] provided a new insight into the atomic arrangement of silicate and aluminate species in hydrated cement pastes. It is argued that in a real cement gel, the aluminum species are mostly octahedral including water molecules and hydroxyl groups in their coordination shell. Based on their NMR observations, Rawal *et al.* suggested that aluminate groups should be at the vicinity of silicate groups. Therefore, it is necessary to provide a molecular description of CASH nano-structure which not only refines available literature but also recent NMR findings.[23,25]

In the present theoretical work mostly inspired by NMR experiments, we explored all the possible set of substitutions. The aluminum incorporation is performed in CSHs of varying C/S ratios. Although the incorporation of aluminum inside the silica chains of low C/S ratio corresponds to the classical tetrahedral coordination of aluminum in many alumino-silicate such as zeolites, substitution of calcium by

L. Struble—contributing editor

Manuscript No. 29842. Received June 08, 2011; approved December 09, 2011.
This work has been supported by the Concrete Sustainability Hub at MIT, with sponsorship provided by the Portland Cement Association (PCA) and the RMC Research & Education Foundation.
[†]Author to whom correspondence should be addressed. e-mail: javad@mit.edu.

aluminum can be viewed as aluminum being located in the interlayer voids of CSHs. In this way of approaching the unknown molecular structure of CASH, we found a consistent picture in which all available structural data are congruently explained. This explanation is quantified through measurement of tetrahedral and octahedral symmetry order parameters in the CASH samples. At a second stage, we paved the first steps toward the application of hierarchical multi-scale modeling connecting the fully discrete atomic scale to the continuous medium in glassy materials.

II. Computational Approach

(1) Force Field

Modeling and Simulation of complex hydrated oxides similar to (ordered) tobermorites and Calcium-Silicate-Hydrate gels require a potential energy model (commonly called force field) that can simultaneously reproduce their mechanical properties and structural configurations. In the force field method, the interactions between different species are described via inter-atomic potential functions that are analytical mathematical expressions. The force field employed in this study uses a combination of Lennard-Jones, Buckigham, Morse, Coulombic and three-body bending terms to construct the potential energy landscape. The calculation of electrostatic interactions between pair of ions is carried out using the three-dimensional Ewald summation method. In addition, the core-shell model is applied to effectively reproduce the polarization of oxygen atoms[27] by using a two-center interaction model made of a core and a shell linked via an elastic spring. The transferability of this force field has been checked with numerous experimental data like[28–31] and quantum mechanical calculations.[32] More specifically, transferability of structural and elastic properties were checked for a large number of systems including a realistic CSH model,[13] tobermorites,[31] lizardite,[29] and heulandite.[28]

(2) Atomistic Simulation of Materials

Different atomistic techniques are applied to the molecular structure of materials to capture their chemo-mechanical properties. We have employed energy minimization, molecular dynamics in different statistical ensembles and grand canonical Monte Carlo (GCMC) for water adsorption. Potential energy minimization to find the local equilibrium ground state energy of the system consists of tracking stationary points that correspond to zero energy gradients with positive curvature on the potential energy hypersurface. Within harmonic approximation of lattice dynamics, the vibration partition function of the system can be calculated from the set of Hessian eigenvalues. Having the partition function, it is then possible to derive all thermodynamic state functions such as system's Gibbs free energy. Given the minimal free energy, the mechanical metrics can be derived from the curvature of free energy landscape.

Molecular dynamics at finite temperature and pressure is performed to relax the atomic structure in NVT and NPT canonical ensembles by integrating equations of motion via Leapfrog Verlet scheme. The temperature and pressure in the system are controlled via Nose-Hoover thermostat and barostat. In the present work, the substitutions are performed in CSH structures with water filling the interlayer spacing and structural voids. Subsequently, we studied whether aluminum substitution changes the water content of the system or not. To accomplish this, grand canonical Monte Carlo simulation is performed which is the appropriate technique to describe water adsorption-desorption in nano-scale porous medium. GCMC simulation in μVT ensemble consists in equilibrating the system at constant temperature, volume, and chemical potential μ that controls the connection of the system to a fictitious reservoir containing an infinite number of water molecules. A single GCMC simulation with the chemical potential of water fixed to the value corresponding to bulk water at the room temperature is performed by considering a core-only model for water oxygen atom and treating the rest of the molecule as a rigid body. In GCMC simulation, Monte Carlo trials are translation, rotation, creation, and destruction of water molecules. All numerical simulations are performed using GULP code.[33,34]

III. Results and Discussion

First, we briefly comment on the morphological structure of CSHs and how it affects the mechanical properties. Given a clarified understanding of CSHs of varying C/S ratio, the effect of substitution of silicon by aluminum is studied afterward. In the third step, we present the morphological and mechanical impacts of substitution of calcium by aluminum. Finally, the coupled chemo-mechanical effect of aluminum incorporation at finite strain in the CSH structures is presented.

(1) Morphology Versus Mechanical Properties of CSH Structures

The calcium to silicon ratio (C/S) plays an important role in CSH structure and its value ranges from 1.2 to 2.3 with the mean value of 1.7.[9] In CSH gels with low calcium content, i.e., low C/S ratio, long silica chains are present. In this C/S regime, the structure of the gel is similar to tobermorite.[5,7,8] As the C/S ratio increases, silica dimmers prevail in the resultant gel. Pellenq *et al.*[13] proposed a consistent CSH model, namely cCSH model, with silica chains of finite size whereas their model was consistent with experimental observations. Three minerals from tobermorite class, 11Å, 14Å and anomalous [Figs. 1(a)–(c)], plus cCSH structure are employed as the structures of CSH at different C/S regimes. Tobermorite 11Å, 14Å and anomalous with C/S ratios of 1, 0.83, and 0.67, respectively, are considered as the minerals which might represent the structure of CSH gel in low C/S ratios. These minerals are made up of parallel octahedral calcium sheets tethered by infinite tetrahedral silica chains. Tetrahedral coordination of silicon species is expressed in terms of the Q^n factor in which the superscript n denotes the number of bridging oxygen atoms attached to a silicon atom [Fig. 1(d)]. While Q^0 denotes the fraction of silica monomers, a silica pentamer has two ending Q^1 (end) sites and three Q^2 (middle) sites. Q^3 and Q^4 silica atoms represent the formation of higher coordination. Considering the position of silicon atom in a finite size silica chain, they can be divided into three classes of bridging, pairing, and ending sites [Fig. 1(e)].

The structural and mechanical properties of CSHs are provided in Table I. Anomalous tobermorite has the highest Ez and it is due to the existence of Q^3 in the crystal which bridges between different layers. Ez of the tobermorite 11Å is higher than that of tobermorite 14Å mainly because of less structural water and thus a lower interlayer distance which increases the interaction of adjacent layers. In addition, the presence of a larger amount of interlayer calcium species (establishing iono-covalent bonds with nonbridging oxygen atoms), makes tobermorite 11Å stronger in basal direction. Despite having lower interlayer spacing, cCSH has the same Ez as tobermorite 14Å due to high water concentration in its interlayer spacing. It is worthwhile to mention that this water has a glassy behavior in this ultra-confining nano-porous medium.[35] The same trend is observed in the indentation modulus except for tobermorite 11Å having larger M than anomalous tobermorite. Indentation modulus represents the volumetric aspects of stiffness rather than a preferential direction. The average elastic modulus in the direction of layers for tobermorite 11Å and anomalous are 107 and 87 GPa, respectively. The high concentration of interlayer calcium plays an important role in increasing the elastic modulus for tobermorite 11Å in the direction of layers. The above reason

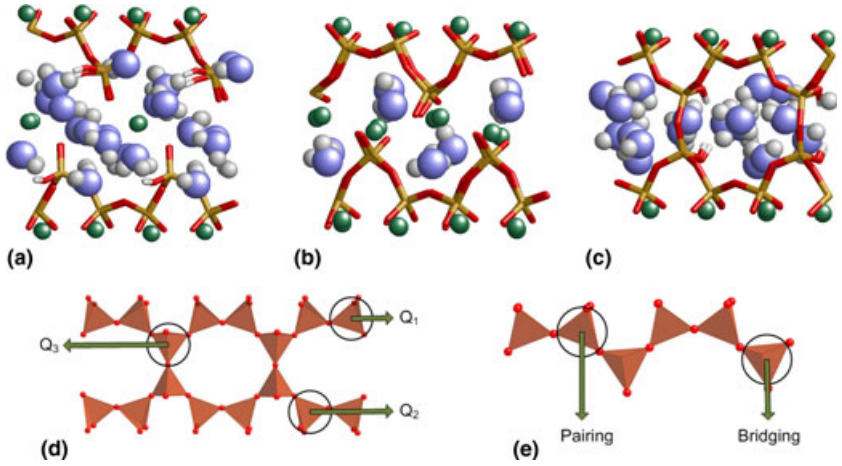

Fig. 1. Structure of tobermorites. (a) tobermorite 14Å (TB14). (b) tobermorite 11Å (TB11). (c) anomalous tobermorite (TBan). The brown-red sticks represent the infinite silica chains. The green spheres are calcium atoms. Oxygen and hydrogen atoms in water molecules are shown by blue and white spheres, respectively. (d) Schematic position of Q^n in an interconnected finite silica chain. N is the number of silica tetrahedral attached to a silica tetrahedral. (e) Bridging and paring sites within an infinite silica chain.

along with higher density and lower water content of tobermorite 11Å justifies its high indentation modulus. The cCSH model has the lowest E_{layer} because of the broken silica chains and existence of voids in the octahedral calcium sheets.

(2) Substitution of Silicon by Aluminum in CSHs

To assess the chemical stability of aluminum substitution, one silicon atom is replaced by an aluminum atom within the silica chains. The charge deficit resulting from this substitution is compensated by adding an extra sodium atom to the interlayer spacing of CSHs. The Al-containing samples are relaxed in NPT ensemble at 300 K and zero external pressure. Subsequently to reach the global minima energy, the samples are relaxed using static energy minimization method at 0 K. A lattice dynamics energy minimization within harmonic approximation theory is performed afterward to calculate the Gibbs free energy at room temperature. As the results in the Table II suggest, the bridging position is more favorable in the structures of lower C/S ratio. This is in agreement with several NMR studies of synthetic CSH gel in presence of sodium atoms claiming that Al substitution is most probable in silica chain bridging sites.[17,20,22] Substitution in the model with high C/S ratio is performed in bridging, pairing, and ending sites of a pentamer silica chain (Fig. 2). The Gibbs free energy as a measure of chemical stability is substantially lower when aluminum substitutes the silica atom in the bridging site. Please note that the embedding energy of silicon atoms varies roughly around 8 eV in the silica chains. This energy difference for aluminum atoms is also affected by the position of charge-neutralizing sodium atoms. Therefore, attaining such an energy difference is not surprising. Moreover, the energy differences between different polymorphs are much higher than thermal energy which means that aluminum is mostly favored in the bridging sites. This is in complete agreement with ^{29}Si and ^{27}Al MAS NMR experiments discarding aluminum in the ending tetrahedral sites.[36–38] Therefore, we exclude the possibility of aluminum being in the pairing sites in high C/S ratios[19,36,39] suggesting it to be mainly in the few bridging sites within silica chains.[17,20,22,40]

Given the chemical stability of the aluminum atom within the CSH structure, the number of substitutions can be increased to study the impact of tetrahedrally coordinated aluminum on the properties of CSH. This together with the nature of the charge-neutralizing counter ion determines the number of all possible systems to be considered in a combinatorial fashion. The combinatorial approach has recently also been applied in modeling impurities in cement clinkers alite and belite.[41] Considering symmetry in the silica chains and relative distance of substitution sites can significantly reduce the number of these possible states. To derive the average mechanical and geometrical observables for a given chemical composition, energy minimization over all possible configurations should be performed. Meanwhile, GCMC sim-

Table I. Atomistic Calculations of Geometrical and Elastic Properties of CSHs with Varying Calcium to Silicon Ratio

Specimen	Height (Å)	Ez (GPa)	E_{layer} (GPa)	Indentation modulus (GPa)
Tobermorite 14Å	14.4	53	76	63
Tobermorite 11Å	12.2	74	107	101
Anomalous tobermorite	11.6	113	87	77
cCSH model	11.8	56	67	65

Table II. The Effect of Incorporation of One Aluminum Atom on CSHs of Lower Calcium to Silicon Ratio (Tobermorite)

Specimen	Position	Height (normalized)	Ez (normalized)	Indentation modulus (normalized)	Free energy (eV)
Tobermorite 14Å	Bridging	1.01	0.94	1.02	E_1
	Pairing	1.01	1.28	1.13	E_1 + 4.8
Tobermorite 11Å	Bridging	1.01	0.97	1.02	E_2
	Pairing	1.01	0.96	1.04	E_2
Anomalous tobermorite	Bridging	1.00	0.96	1.14	E_3
	Pairing	1.00	0.97	1.10	E_3 + 0.5

Sodium atoms are used for charge-neutralization and mechanical properties are normalized with respect to their pure structure.

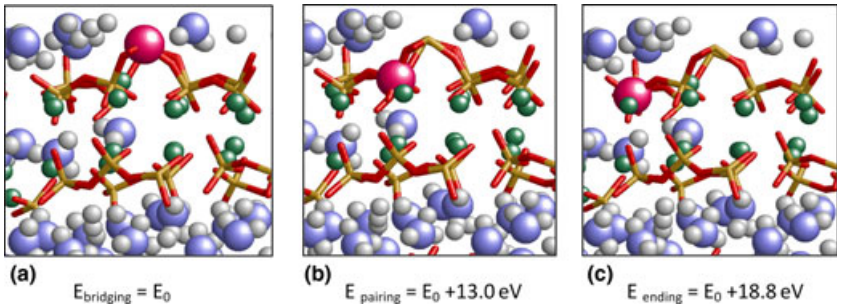

Fig. 2. Stability of aluminum atom within a finite size silica chain within a realistic environment. Silicon is structurally substituted by aluminum atom in the (a) bridging, (b) pairing, and (c) ending sites of a pentameric silica chain. The aluminum atoms are represented by large pink spheres. Thermodynamically aluminum atom is favored in the bridging position rather than at the other two replacement sites.

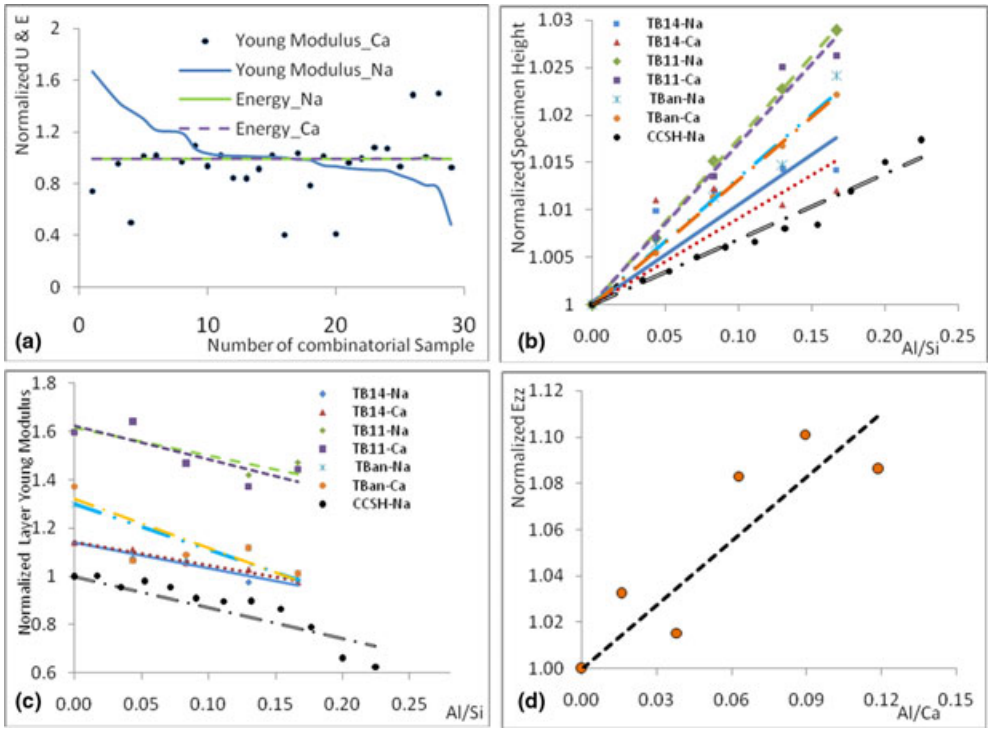

Fig. 3. The effect of Aluminum substitution on the mechanical properties of CSHs of varying calcium to silicon ratios using combinatorial analysis approach over more than 20 000 atomistic models. (a) Normalized energy (U) and elastic modulus (E) for substitution of two aluminum atoms within the infinite silica chains of tobermorite 11Å. (b) Variation of cell dimension (height) in the direction perpendicular to the silica chains. Generally, insertion of charge-neutralizing agents increases the interlayer spacing. (c) Average elastic modulus of calcium-silicate layers by aluminum content in the silica chains with normalization by the elastic modulus of cCSH model. (d) The elastic modulus in the direction perpendicular to silica chains in the substitution of calcium by aluminum. TB14, tobermorite 14Å; TB11, tobermorite 11Å; TBan, Anomalous tobermorite.

ulation of water adsorption (with the water chemical potential set to that of the bulk liquid at room temperature) is performed over a number samples to verify that the presence of aluminum does not alter the water content of the structures compared to the aluminum-free reference system. The mechanical observable at a given chemistry is the average of that parameter in each state times its Boltzmann probability. The normalized energy and Young modulus for two substitutions in tobermorite 11Å using both sodium and calcium neutralizing counter-ions are presented in Fig. 3(a). While all the atomic configurations are energetically competing (polymorphs), It is interesting to note that the mechanical properties can significantly vary showing a strong dependence not only on the configuration of aluminum atoms in the chain but also on the counter-ion used to charge-neutralize the system. From the equality of internal energy, it can be inferred that all polymorphs are equally probable; any observable property can be simply averaged among them. Given the notion of equi-probability of states, about 6000 models are built with different aluminum content and charge neutralizers (Ca^{++} & Na^{+}). These models are analyzed hereafter to study the response of tobermorite structures for a same chemical composition. For the case of cCSH model, the aluminum substitution is increased gradually to all the possible sites.

The effect of aluminum content on the simulation cell height, twice the basal distance, of the tobermorite minerals and cCSH structure is presented in Fig. 3(b). Each value is normalized with respect to its corresponding height in Table I. It is found that the average height of the aluminum-substituted minerals is not affected by the type of charge-balancing agent. Although the sample height increases with the aluminum content, the density remains almost the same due to insertion of charge-balancing cations. Therefore, it does not lead to a variation in the water content compared to the aluminum-free reference as shown from GCMC simu-

lations. Interestingly, the behavior of tobermorite 14Å in the basal direction is fairly complex. It is worth recalling that this tobermorite has the largest basal distance in all tobermorite minerals and water content implying a shielding hydration effect of interlayer ions. These two structural characteristics limit the effect of cations on increasing samples height. tobermorite 11Å, anomalous tobermorite, and cCSH model have roughly the same basal distance and therefore their response should be similar to each other. The large water content of the cCSH model (in agreement with experiments) prevents charge-balancing cations to fully interact with silica atoms in the chains. This mitigates the effective expansion of the layers which causes the cCSH model to have a lowest slope. Presence of Q^3 sites in the structure of anomalous tobermorite constrains its free deformation in the basal direction.

The structural changes induced by silicon-aluminum substitution entails notable impacts on the mechanical properties of this type of CASH structures which are presented in Fig. 3(c). By increasing the aluminum content and regardless of C/S ratio and counter-ion used, the average elastic modulus of calcium-silicate layers is reduced notably meaning that the incorporation of aluminum weakens the material's stiffness. It means that alumino-silicate tetrahedral chains are not as strong as pure silica chains. All other mechanical metrics decrease with increasing aluminum content inside the chains. Formation of local charge defects by insertion of aluminum atoms in the silica chains is followed by rearrangement of cations and water molecules around the substitution sites. The locally charged unbalanced environment around aluminum atoms attracts charge compensation alkali agents toward the substitution site which pairs aluminum and sodium atoms together within 3–4 Å although these are of same (+) electrical charge hence subject to a priori columbic repulsion that is mitigated by the presence of negative oxygen species in their immediate neighborhood. The water molecules in the interlayer regions rotate in a way to expose hydrogen atoms to the aluminum species and place them ~3 Å apart. Consequently, to maintain the internal structure of water molecules, oxygen atoms stay further away from aluminum atoms to place them in a relative distance of ~4 Å. This justifies the observed proximity of OH groups closed to the aluminate species observed in the recent NMR experiments.[23]

(3) Substitution of Calcium by Aluminum in CSH

The disordered structure of cCSH makes possible the substitution of interlayer calcium atoms with aluminum atoms (typically two Aluminum ions substituting three Calcium ions). The incorporation of aluminum in the interlayer regions of CSH is followed by immense internal reconfiguration that directly affects the mechanical response of the atomic structure Fig. 4. As displayed in Figs. [4(a)–(c)], by introducing aluminum to the interlayer spacing by substituting calcium ions, we found the evidence of a "healing" process: the aluminum species diffuses from its original calcium site to a vacant tetrahedral site in-between silica chain chunks. This fact is explicitly shown by an extremely sharp peak at 1.9 Å in the aluminum-oxygen pair distribution function [see Figs. 5(a) and (c)] which is quite comparable to that of substitution of silicon by aluminum. This peak can be cap-

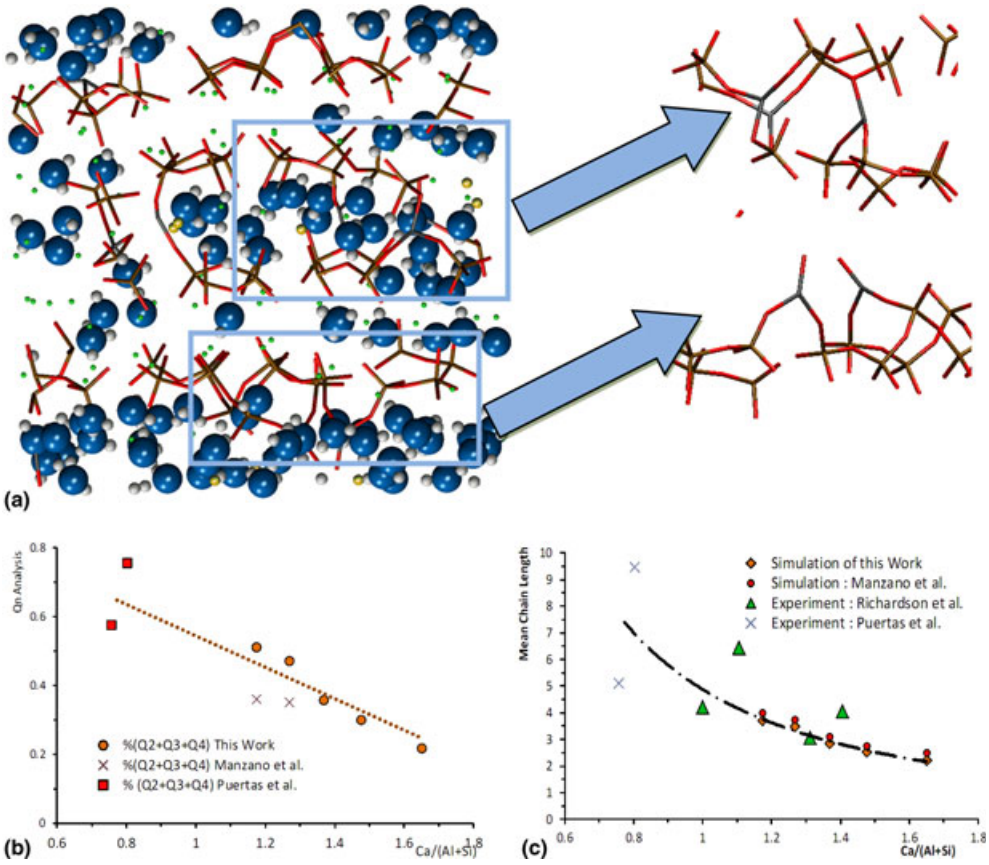

Fig. 4. Combinatorial analysis of aluminum-calcium substitution and its effect on the structure of calcium-silicate-hydrates at high calcium to silicon ratios. (a) The sample structure of calcium-aluminate-silicate produced by calcium-aluminum substitution and neutralized with sodium alkali agents. (b) Formation of Complex three-dimensional alumino-silicate skeletons connecting silica monomers and dimmers between adjacent layers. (c) Formation of longer silica chains by aluminum-connecting adjacent dimmers. (d) Variation of Q^n sites by increasing Al/Ca ratio. A linear reduction in the amount of monomer and dimmers is followed by increase in the polymerization of silica chains. (e) The effect of aluminum content on the mean chain length.

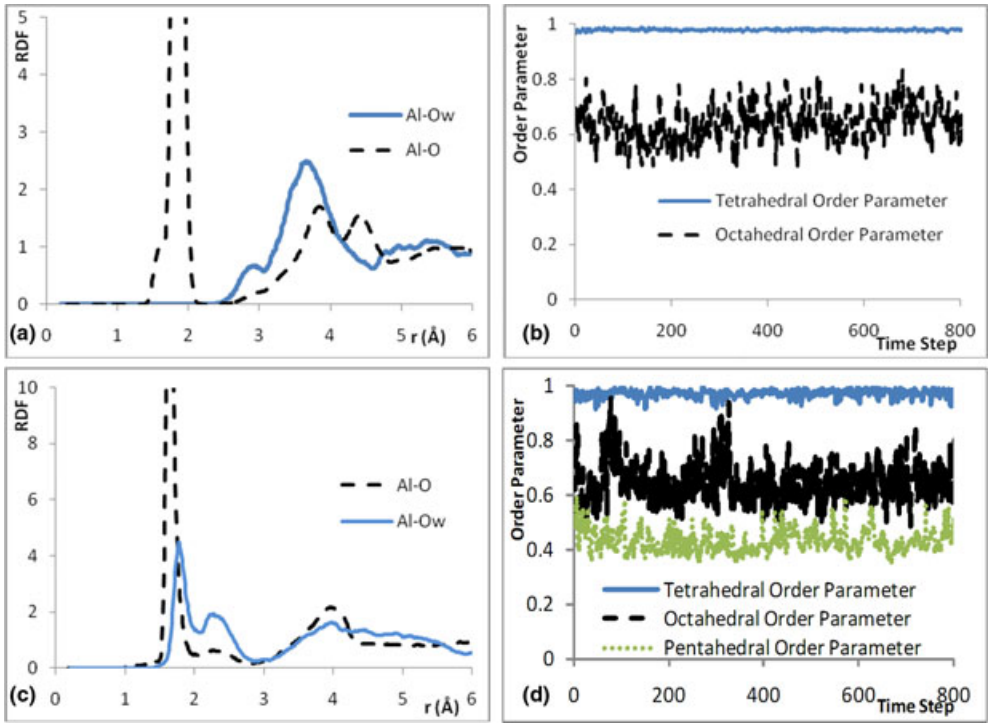

Fig. 5. Radial Distribution Function, tetrahedral and octahedral order parameter. (a) Radial distribution function for Aluminum-Oxygen in a silicon substituted sample. (b) Aluminum order parameter in aluminum-silicon substitution case. Since Aluminum is substituted inside the chains, they are exhibiting tetrahedral coordination. (c) Radial distribution function for Aluminum-Oxygen substitution in a calcium substituted sample. (d) Aluminum order parameter in aluminum-calcium substitution case.

tured using clayff force field as well. Since CSH has an iono-covalent structure, the columbic forces are dominant in the evolution of the system in phase space. Due to this nature, both core-shell and clayff force fields can correctly capture reconfiguration of aluminum atoms but they cannot capture the condensation energy related to the formation and breakage of bonds. Therefore, the disassociation of water molecule to form hydroxyl groups cannot be studied via core-shell force field. This requires the use of first principle *ab initio* calculations via DFT method which is computationally nearly intractable for systems as large as cCSH. The calculation of condensation energy for the silica chains of a few atoms was performed by Manzano *et al.*[42] which revealed this energy is in the order of 1 eV which is a small fraction of columbic energy.

The aluminum-calcium substitution process is way beyond the mere existence of aluminum in the interlayer spacing suggested by other authors.[16,17] The suggested healing effect of aluminum-calcium substitution is that the aluminum atoms bridge between silica chains to form an alumino-silicate chains network with different types of coordination based on chains healing and leading to one-dimensional or/and two-dimensional or/and three-dimensional chain linkages. This phenomenon increases the integrity of the CSH structure producing a pathway to transfer internal stress field through strong and chemically stable formations.

The GCMC simulations again confirm that water content does not change by substitution of calcium by aluminum. As described in Fig. 4(b), as aluminum substitutes calcium and Ca/(Al + Si) ratio decreases, the percentage of $(Q^2 + Q^3 + Q^4)$ increases while the $(Q^0 + Q^1)$ decreases. A detailed distribution of Q^n sites as function of Ca/(Al + Si) ratio is provided in Table III. This matches well with the formation of alumino-silicate glasses using reactive force field modeling by Manzano *et al.*[43] This theoretically explains the formation of alumino-silicate networks observed in NMR experiments[20,36] which indicates the increase of the Q^2 (1Al) signal and the appearance of a Q^3 (1Al) peak. The mean chain length as a measure of polymerization of silica chain is calculated accordingly [Fig. 4(c)]. This parameter has been closely related to the creep and durability of concrete structures. In fact, the gradual viscoelastic deformation of CSH-based materials coincides with polymerization of silica chains during its meta-stable hydration process. Roughly, by a 10% increase in the aluminum content in the interlayer of CSH structure which is equal to 45% decrease in Ca/(Al + Si) ratio, the mean chain length is increased by 85%. These results are in good agreement with the separate NMR experiments of Puertas *et al.*[44] and Richardson *et al.*[45], and polymerization simulations of Manzano *et al.*[43] Although NMR experimentalists attribute the increase in chain length to the silicon-aluminum substitution[16,17] only, we highlight that this phenomenon is probably due to calcium-aluminum replacements. The possibility of cross-links between layers (Q^3 sites giving rise to a three-dimensional solid) can influence the way load is transferred from one layer to the next. To investigate the effect of geometrical transformations to the mechanical observables of the system, the normalized Young modulus in the direction perpendicular to the calcium-silicate layers is plotted versus the aluminum content [Fig. 3(d)]. The Young modulus in the weakest direction linearly increases with Al/Ca ratio confirming the strong correlation between geometry and mechanics of CASH nanocomposites. In addition, the recent work of Puertas *et al.* suggests that the nano-scale porosity and type of activator play a crucial role in the final mechanical properties at micrometer scales.

To quantitatively assess the coordination of aluminum atoms within these samples, the order parameter is calculated over molecular dynamics trajectories. Although the tetrahedral order parameter has been extensively used in the literature, we propose a simple practical relation for evaluating penta-/octahedral parameters. These order parameters are calculated using the following relations:

Table III. The Percentage of Q^n and Mean Chain Length in CASH of Varying Chemistry Calculated via Molecular Modeling

Ca/(Al + Si)	Q^0, %	Q^1, %	Q^2, %	(Q^3 + Q^4), %	MCL
1.7	0.12	0.67	0.21	0.0	2.2
1.5	0.09	0.61	0.28	0.02	2.5
1.4	0.06	0.58	0.33	0.03	2.8
1.3	0.05	0.48	0.41	0.06	3.5
1.2	0.05	0.44	0.44	0.07	3.7

$$OP_{tetra} = \langle 1 - \frac{3}{8}\sum_{\mathbf{i}}\sum_{\mathbf{j}}\left[(\cos\theta_{\mathbf{ij}})^2 + \frac{1}{3}\right]\rangle \quad (1)$$

$$OP_{octa} = \langle \sum_{\mathbf{i}}\sum_{\mathbf{j}}\left[(\cos\theta_{\mathbf{ij}})^2\right] - 2\rangle \quad (2)$$

$$OP_{penta} = \langle \sum_{\mathbf{i}}\sum_{\mathbf{j}}\left[(\cos\theta_{\mathbf{ij}})^2\right] - \frac{3}{4}\rangle \quad (3)$$

where **i** and **j** are the summations over Al–O bonding spatial vectors. More importantly, **i** and **j** vectors should be within the first shell of neighbors which is identified by Radial Distribution Functions (RDF). The above octahedral order parameter is checked for corundum mineral which gives the value of 1 for octahedrally coordinated aluminum atoms. A complete set of RDF and order parameter calculations is presented in Fig. 5. For the case of silicon substitution by aluminum, the first shell of oxygen atoms are located within the distance of 1.9 Å from aluminum atoms [Fig. 5(a)]. In such a substitution, the tetrahedral order parameter is 0.98 ± 0.01 which apparently shows that aluminum is tetrahedrally coordinated. By additionally considering the first shell of oxygen atoms from water molecules, the octahedral order parameter value is 0.57 ± 0.07 [Fig. 5(b)] that compares well with the octahedral order parameter value for (pseudo) octahedrally coordinated calcium atoms in tobermorite minerals 0.55 ± 0.02. The term "pseudo" is introduced as some Ca in tobermorite layers are in fact sevenfold coordinated.[8] However, these water molecules are quite far away from substitution sites (around 4 Å) i.e., in the range of a second shell of substrate oxygen neighbors [Fig. 5(a)]. So Al substituting Si sites cannot be considered as really being in an octahedral environment when considering closest water molecules; by contrast, they are clearly tetrahedrally coordinated.

In the case of aluminum substituting calcium, aluminum atoms migrate close to oxygen atoms which also give a peak in the 1.9 Å in RDF diagram [Fig. 5(c)]. A few atoms get fully tetrahedrally coordinated. In addition, water molecules can get very close to the aluminum atoms [Fig. 5(c)]. This leads to a strong octahedral signal which is shown by octahedral order parameter of 0.64 ± 0.07 and a poor pentahedral signal of 0.45 ± 0.06. We recall that the octahedral order parameter value for (pseudo) coordinated calcium atoms in tobermorite sheets is 0.55 ± 0.0.2. Therefore, by considering water molecules, an octahedral signal can be observed (Fig. 6). The aluminum's octahedrality is even more than the octahedral order parameter of calcium atoms in the tobermorite. The weak pentahedral order parameter is due to distortion of five neighboring oxygen atoms around aluminum sites. The ratio of octahedral to pentahedral aluminum sites is measured to be roughly 3 in the molecular models although deconvolution of NMR spectrum for hardened Portland cement paste is about 3.5.[23] This clearly shows the multifarious behavior of aluminum atoms in the calcium-aluminate-silicate-hydrates in which aluminum can exhibit both tetrahedral and octahedral signals if one considers two different types of substitutions. These results are fully consistent with the set of solid state ^{27}Al and ^{29}Si NMR data published in literature and specially the recent work of Rawal *et al.*[23] and Andersen *et al.*[25] The qualitative molecular structure presented by Rawal *et al.*[23] shows that tetra-/penta-/octahedral coordination of aluminum atoms is due to arrangement of water molecules around aluminum atoms which is in complete agreement with what we found here.

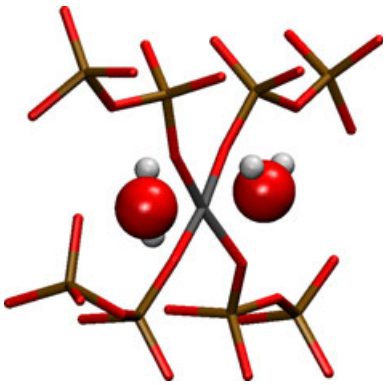

Fig. 6. Octahedral coordination of aluminum atoms. In this case, aluminum atom has reorganized itself with four oxygen atoms of four neighboring silica dimmers. In addition, two water molecules have rearranged themselves at either sides of the Al–O plain. Totally, six oxygen atoms have surrounded the aluminum atom producing an octahedral coordination.

Despite the assertion in[16] regarding the inclusion of aluminum within the core of octahedral calcium layers, we emphasize that such a substitution is physically impossible. This fact can be readily understood in the context of Al–O bond length which is much smaller than that of Ca–O and incorporation of aluminum in such layers leads to structural instability. Andersen *et al.*[25] provide the same structural reason to discard aluminum from main calcium layers. Therefore, the octahedral coordination is either due to coordination of aluminum to the oxygen atoms (from silica chains and water molecules) in the interlayer space as explained above or to other hydration products such as ettringite, hydrogarnet, monosulphate, and other aluminate hydrates.[24]

(4) Deformation and Multi-Scale Response of CASHs Versus CSHs

The equilibrium combinatorial analysis is pursued by a mechanistic study on the deformation and failure mechanisms in CSH and CASH structures. To unravel the chemo-mechanical effect of aluminum substitutions, both types of aluminum-enriched CASHs with the same substitution degree are directly compared with defect-free tobermorite 14Å and cCSH structures. All structures are relaxed in NPT ensemble at room temperature and zero external pressure and equilibrated using static energy minimization at constant pressure to reach the potential energy minima and remove all internal stresses. The deformation is subsequently applied in a manner similar to deformation gradient defined in the mechanics of continuous medium. In classical continuum mechanics, the deformation gradient is a second order tensor that maps an infinitesimal vector d**X** in the material configuration to its counterpart d**x** in the spatial configuration as:

$$dX_{\mathbf{i}} = F_{\mathbf{ij}}\, dx_{\mathbf{j}} \quad (4)$$

where $\mathbf{F_{ij}}$ is the partial derivative $\frac{\partial X_i}{\partial x_j}$ in Cartesian coordinate.[46] In simple shear deformation, the deformation gradient tensor is defined as:

$$F = \begin{bmatrix} 1 & \tan\theta & 0 \\ 0 & 1 & 0 \\ 0 & 0 & 1 \end{bmatrix} = \begin{bmatrix} 1 & \alpha & 0 \\ 0 & 1 & 0 \\ 0 & 0 & 1 \end{bmatrix} \quad (5)$$

where α and θ represent the shear number and angle, respectively. Due to the nonlinear nature of interatomic forces, the large strain deformations are easily dealt with in an updated-Lagrangian fashion. Here, 50 strain increments each 0.002 in magnitude are imposed to the structures. After each strain increment, the samples are relaxed via constant volume energy minimization to capture the nonlinear behavior of atomic system in a displacement-controlled fashion. Here, the results of a shear deformation are presented (Fig. 7).

The elastic responses of Al-containing samples range between two extremes: defective cCSH and pure tobermorite mineral [Fig. 7(a)]. In aluminum-silicon CASH models, population of alkaline or alkaline earth agents in the interlayer reinforces the interaction between different layers leading to a higher strength of the material. The formation of three-dimensional alumino-silicate network further increases the strength and elastic response of the aluminum replacing calcium CASH structures. The results of this analysis corroborate the aforementioned partial healing mechanism produced by aluminum. The increase in the interlayer interactions and substantial improvement in the mechanical response of calcium-silicate layers is also observed in other deformation paths.

To quantitatively study the kinematics of deformation in the CASH structures, root mean square deviation from linear elastic deformation (RMSDLED) is calculated. RMSDLED is a multi-scale metric for measuring the deviation of molecular structures from kinematic linear Cauchy–Born hypothesis.[47] The Cauchy–Born (CB) hypothesis is a homogenization assumption in the molecular theory of elasticity in which the atomic positions are related to the continuum field through the deformation gradient F [see Eq. (3)]. The well-known CB hypothesis assumes that if the boundaries of a defect-free infinite crystalline lattice are subjected to a homogeneous deformation, the entire lattice deforms according to the above-mentioned deformation gradient.[47] From the energetic point of view, the CB hypothesizes that the linear deformation of the lattice minimizes the free energy of the crystal. In fact, the CB hypothesis can be employed wherever a description of underlying atomic structure is available. This issue has been recently investigated[47,48] to derive grounds for the CB hypothesis and has led to a validity criterion of CB

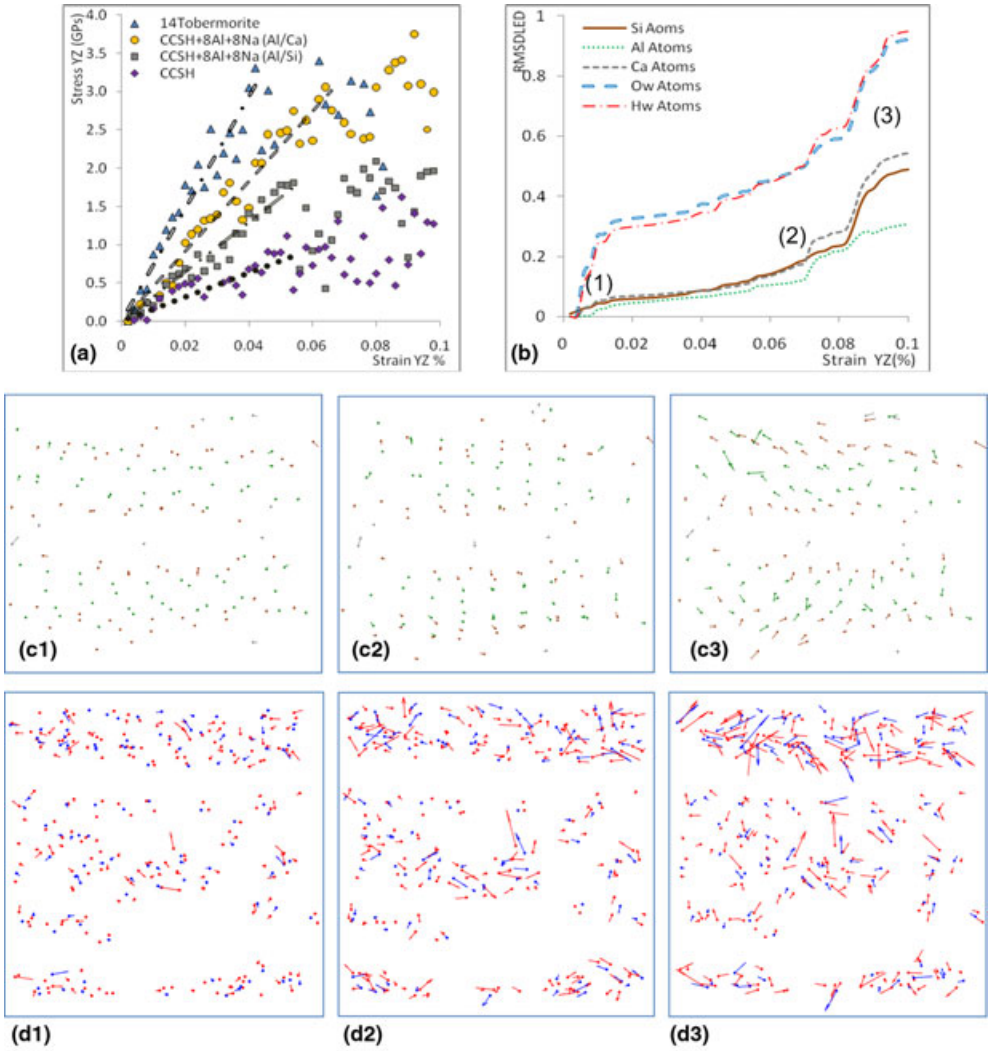

Fig. 7. (a) Stress-strain diagram for cCSH, tobermorite 14 and two different types of CASH. In one sample aluminum atoms have substituted silicon whereas in the other the same number of atoms have substituted calcium. (b) Evolution of root mean square deviation from linear elastic deformation for different elements in the sample with eight aluminum atoms substituting the calcium atoms in the interlayer. (c) Three sequences of deviation vector for silicon, calcium and aluminum atoms. (d) Three sequences of deviatoric motion from linear elastic deformation for water molecules. The color definition in the vector plots are the same as RMSDLED diagram.

hypothesis using a comparative investigation from the atomistic and continuous models, in which the crystalline lattice deforms homogeneously.

This hypothesis has been successfully implemented in multi-scale modeling of defects,[49] nano-indentation,[50] fracture,[51] grain boundaries,[52] and surface stress[53] in crystalline solids. The difference between the deformations predicted by means of CB and the exact solution derived by means of discrete lattice statics energy minimization reads:

$$\mathrm{RMSDLED} = \sqrt{\frac{1}{3N-1}\sum_{i=1,}^{N}(r_{\mathrm{CB}} - r_{\mathrm{EM}})^2} \qquad (6)$$

The root mean square deviation from Cauchy–Born hypothesis in strain field is defined in Eq. (6) where N is the total number of a certain type of atoms, $\mathbf{r}_{\mathrm{EM}}$ is the spatial vector of i*th* atom derived by means of energy minimization method at a certain level of deformation and $\mathbf{r}_{\mathrm{CB}}$ is the spatial vector of i*th* atom predicted by means of Cauchy–Born hypothesis. In fact, RMSDLED can determine the state in which the irreversible deformation occurs due to a small perturbation in the discrete system.

The deviation is caused by nonlinearity of interatomic interactions, geometrical arrangement of the structure or failure mechanisms. The results of Fig. 7(b) indicate that the kinematics of water molecules should be distinguished from that of calcium-alumino-silicate skeletal species. In the early stages of the deformation, the water molecules flow in random directions within the interlayer. It means that the motion of water molecules in the interlayer spacing does not obey the Cauchy–Born hypothesis. Thus, this theory is not applicable for heterogeneous hydrated materials similar to CSH. Although most of the water molecules experience this free motion, deformation of ultra-high confined water molecules within cavities inside the layers (this is one of the main features of the cCSH model[13]) obey this hypothesis. The solid skeletal species motion gradually deviates from homogeneous deformation over the course of displacement which is explained by the nonlinear nature of interactions and geometrical features of the CASH glassy structures. Between the second and the third stages [Figs. 7(c)–(d)], CASH undergoes a localized shear deformation within the solid layers. This irreversible deformation can be viewed as the formation of a counter clockwise vortex in the calcium-alumino-silicate shown in arrow diagrams. This was observed in shear deformation of metals.[48] Therefore, it can at least be concluded that Cauchy-Born hypothesis can be applied in small deformation regimes in the single phase solid heterogeneous materials similar to dried gels with entrapped water in the nano-pores of the nano-porous medium. This sets the roots for the applications of multi-scale modeling of mechanical properties of complex hydrated oxides.

IV. Conclusion

In summary, we have identified two ways for substituting aluminum in layered CSH: the aluminum-silicon substitution which is common in alumino-silicate minerals and the calcium-aluminum substitution. More precisely, the silicon-aluminum substitution is favored in bridging sites of silica chains only (excluding all ending sites) whereas the calcium to aluminum substitution leads to the diffusion of aluminum atoms to vacant silica tetrahedral sites. This concerns only the interlayer calcium content (the intralayer calcium species cannot be substituted by aluminum). The consequence of interlayer calcium ions substitutions by aluminum is a healing process that allows the lengthening of silica chains and cross-linkages between layers leading to improved mechanical properties that impact CASH durability. In case of aluminum-calcium substitution, study of the penta-/octahedral order parameter revealed that the aluminum can have penta-/octahedral coordination because of the nearby arrangement of water molecules which is fully consistent with the most recent solid state NMR data available.[23] Finally, we paved the first steps toward the application of the multi-scale Cauchy–Born theory for the nanotexture of cementitious materials. In particular we were able to identify a localized shear deformation within the solid layers.

References

[1]J. Skibsted, H. J. Jakobsen, and C. Hall, "Direct Observation of Aluminum Guest Ions in the Silicate Phases of Cement Minerals by Al-27 Mas NMR-Spectroscopy," *J. Chem. Soc.-Faraday Trans.*, **90** [14] 2095–8 (1994).

[2]H. F. H. F. W. Taylor, *Cement Chemistry*, 2nd edition, Thomas Telford, London, UK, 1997.

[3]A. J. Allen, J. J. Thomas, and H. M. Jennings, "Composition and Density of Nanoscale Calcium-Silicate-Hydrate in Cement," *Nat. Mater.*, **6** [4] 311–6 (2007).

[4]F. J. Ulm, A. Delafargue, and G. Constantinides, "Experimental Micropo-romechanics"; pp. 207–88 in *Applied Micromechanics of Porous Materials*, Edited by L. Dormieux and F. J. Ulm. Springer, New York, 2005.

[5]S. A. Hamid, "The Crystal-Structure of the 11-a Natural Tobermorite $Ca_{2.25}[Si_3o_{7.5}(OH)_{1.5}]\cdot 1H_2O$," *Z. Kristall.*, **154** [3–4] 189–98 (1981).

[6]P. Faucon, J. M. Delaye, J. Virlet, J. F. Jacquinot, and F. Adenot, "Study of the Structural Properties of the C-S-H(I) by Molecular Dynamics Simulation," *Cem. Concr. Res.*, **27** [10] 1581–90 (1997).

[7]S. Merlino, E. Bonaccorsi, and T. Armbruster, "The Real Structure of Tobermorite 11 Angstrom: Normal and Anomalous Forms, Od Character and Polytypic Modifications," *Eur. J. Mineral.*, **13** [3] 577–90 (2001).

[8]T. Mitsuda and H. F. W. Taylor, "Normal and Anomalous Tobermorites," *Mineral. Mag.*, **42** [322] 229–35 (1978).

[9]I. G. Richardson, "The Nature of C-S-H in Hardened Cements," *Cem. Concr. Res.*, **29** [8] 1131–47 (1999).

[10]X. D. Cong and R. J. Kirkpatrick, "Si-29 Mas Nmr Study of the Structure of Calcium Silicate Hydrate," *Adv. Cem. Based Mater.*, **3** [3–4] 144–56 (1996).

[11]H. F. W. Taylor, "Proposed Structure for Calcium Silicate Hydrate Gel," *J. Am. Ceram. Soc.*, **69** [6] 464–7 (1986).

[12]A. Nonat, "The Structure and Stoichiometry of C-S-H," *Cem. Concr. Res.*, **34** [9] 1521–8 (2004).

[13]R. J. M. Pellenq, A. Kushima, R. Shahsavari, K. J. Van Vliet, M. J. Buehler, S. Yip, and F. J. Ulm, "A Realistic Molecular Model of Cement Hydrates," *Proc. Natl. Acad. Sci. USA*, **106** [38] 16102–7 (2009).

[14]H. Stade and D. Muller, "On the Coordination of Al in Ill-Crystallized C-S-H Phases Formed by Hydration of Tricalcium Silicate and by Precipitation Reactions at Ambient-Temperature," *Cem. Concr. Res.*, **17** [4] 553–61 (1987).

[15]H. Stade and W. Wieker, "On the Structure of Ill-Crystallized Calcium Hydrogen Silicates .3. Incorporation of Al-3+ Ions Into C-S-H(Di,Poly), and Formation of an Instable 11-a Tobermorite," *Z. Anorg. Allg. Chem.*, **494** [11] 179–88 (1982).

[16]P. Faucon, A. Delagrave, J. C. Petit, C. Richet, J. M. Marchand, and H. Zanni, "Aluminum Incorporation in Calcium Silicate Hydrates (C-S-H) Depending on Their Ca/Si Ratio," *J. Phys. Chem. B*, **103** [37] 7796–802 (1999).

[17]M. D. Andersen, H. J. Jakobsen, and J. Skibsted, "Incorporation of Aluminum in the Calcium Silicate Hydrate (C-S-H) of Hydrated Portland Cements: A High-Field Al-27 and Si-29 Mas Nmr Investigation," *Inorg. Chem.*, **42** [7] 2280–7 (2003).

[18]C. R. A. Catlow, A. R. George, and C. M. Freeman, "Ab Initio and Molecular-Mechanics Studies of Aluminosilicate Fragments, and the Origin of Lowenstein's Rule," *Chem. Commun.*, [11] 1311–2 (1996).

[19]P. Faucon, J. C. Petit, T. Charpentier, J. F. Jacquinot, and F. Adenot, "Silicon Substitution for Aluminum in Calcium Silicate Hydrates," *J. Am. Ceram. Soc.*, **82** [5] 1307–12 (1999).

[20]G. K. Sun, J. F. Young, and R. J. Kirkpatrick, "The Role of Al in C-S-H: Nmr, Xrd, and Compositional Results for Precipitated Samples," *Cem. Concr. Res.*, **36** [1] 18–29 (2006).

[21]M. D. Andersen, H. J. Jakobsen, and J. Skibsted, "Characterization of White Portland Cement Hydration and the C-S-H Structure in the Presence of Sodium Aluminate by Al-27 and Si-29 Mas Nmr Spectroscopy," *Cem. Concr. Res.*, **34** [5] 857–68 (2004).

[22]X. Pardal, I. Pochard, and A. Nonat, "Experimental Study of Si-Al Substitution in Calcium-Silicate-Hydrate (C-S-H) Prepared Under Equilibrium Conditions," *Cem. Concr. Res.*, **39** [8] 637–43 (2009).

[23]A. Rawal, B. J. Smith, G. L. Athens, C. L. Edwards, L. Roberts, V. Gupta, and B. F. Chmelka, "Molecular Silicate and Aluminate Species in Anhydrous and Hydrated Cements," *J. Am. Chem. Soc.*, **132** [21] 7321–37 (2010).

[24]P. Meredith, A. M. Donald, N. Meller, and C. Hall, "Tricalcium Aluminate Hydration: Microstructural Observations by In-Situ Electron Microscopy," *J. Mater. Sci.*, **39** [3] 997–1005 (2004).

[25]M. D. Andersen, H. J. Jakobsen, and J. Skibsted, "A New Aluminium-Hydrate Species in Hydrated Portland Cements Characterized by Al-27 and Si-29 Mas Nmr Spectroscopy," *Cem. Concr. Res.*, **36** [1] 3–17 (2006).

[26]I. G. Richardson, "The Nature of the Hydration Products in Hardened Cement Pastes," *Cem. Concr. Compos.*, **22** [2] 97–113 (2000).

[27]B. G. Dick and A. W. Overhauser, "Theory of the Dielectric Constants of Alkali Halide Crystals," *Phys. Rev.*, **112** [1] 90–103 (1958).
[28]A. R. Ruiz-Salvador, A. Gomez, D. W. Lewis, G. Rodriguez-Fuentes, and L. Montero, "Silicon-Aluminium Distribution in Dehydrated Calcium Heulandite," *PCCP Phys. Chem. Chem. Phys.*, **1** [7] 1679–85 (1999).
[29]A. L. Auzende, R. J. M. Pellenq, B. Devouard, A. Baronnet, and O. Grauby, "Atomistic Calculations of Structural and Elastic Properties of Serpentine Minerals: The Case of Lizardite," *Phys. Chem. Miner.*, **33** [4] 266–75 (2006).
[30]C. I. Sainz-Diaz, A. Hernández-Laguna, and M. T. Dove, "Modeling of Dioctahedral 2:1 Phyllosilicates by Means of Transferable Empirical Potentials," *Phys. Chem. Miner.*, **28** [2] 130–41 (2001).
[31]H. Manzano, J. S. Dolado, and A. Ayuela, "Elastic Properties of the Main Species Present in Portland Cement Pastes," *Acta Mater.*, **57** [5] 1666–74 (2009).
[32]K. P. Schroder and J. Sauer, "Potential Functions for Silica and Zeolite Catalysts Based on Ab Initio Calculations .3. A Shell Model Ion Pair Potential for Silica and Aluminosilicates," *J. Phys. Chem.*, **100** [26] 11043–9 (1996).
[33]J. D. Gale and A. L. Rohl, "The General Utility Lattice Program (Gulp)," *Mol. Simul.*, **29** [5] 291–341 (2003).
[34]J. D. Gale, "Gulp: A Computer Program for the Symmetry-Adapted Simulation of Solids," *J. Chem. Soc.-Faraday Trans.*, **93** [4] 629–37 (1997).
[35]M. Youssef, R. J. M. Pellenq, and B. Yildiz, "Glassy Nature of Water in an Ultraconfining Disordered Material: The Case of Calciumâ''Silicateâ''Hydrate," *J. Am. Chem. Soc.*, **133** [8] 2499–510 (2011).
[36]S. Komarneni, R. Roy, D. M. Roy, C. A. Fyfe, G. J. Kennedy, A. A. Bothnerby, J. Dadok, and A. S. Chesnick, "Al-27 and Si-29 Magic Angle Spinning Nuclear Magnetic-Resonance Spectroscopy of Al-Substituted Tobermorites," *J. Mater. Sci.*, **20** [11] 4209–14 (1985).
[37]P. Faucon, T. Charpentier, A. Nonat, and J. C. Petit, "Triple-Quantum Two-Dimensional Al-27 Magic Angle Nuclear Magnetic Resonance Study of the Aluminum Incorporation in Calcium Silicate Hydrates," *J. Am. Chem. Soc.*, **120** [46] 12075–82 (1998).
[38]J. Schneider, M. A. Cincotto, and H. Panepucci, "Si-29 and Al-27 High-Resolution Nmr Characterization of Calcium Silicate Hydrate Phases in Activated Blast-Furnace Slag Pastes," *Cem. Concr. Res.*, **31** [7] 993–1001 (2001).
[39]P. Faucon, T. Charpentier, D. Bertrandie, A. Nonat, J. Virlet, and J. C. Petit, "Characterization of Calcium Aluminate Hydrates and Related Hydrates of Cement Pastes by Al-27 Mq-Mas Nmr," *Inorg. Chem.*, **37** [15] 3726–33 (1998).
[40]I. G. Richardson, A. R. Brough, R. Brydson, G. W. Groves, and C. M. Dobson, "Location of Aluminum in Substituted Calcium Silicate Hydrate (C-S-H) Gels as Determined by Si-29 and Al-27 Nmr and Eels," *J. Am. Ceram. Soc.*, **76** [9] 2285–8 (1993).
[41]H. Manzano, E. Durgun, M. J. Abdolhosseine Qomi, F.-J. Ulm, R. J. M. Pellenq, and J. C. Grossman, "Impact of Chemical Impurities on the Crystalline Cement Clinker Phases Determined by Atomistic Simulations," *Cryst. Growth Des.*, **11** [7] 2964–72 (2011).
[42]H. Manzano, J. S. Dolado, and A. Ayuela, "Aluminum Incorporation to Dreierketten Silicate Chains," *J. Phys. Chem. B*, **113** [9] 2832–9 (2009).
[43]H. Manzano, J. S. Dolado, M. Griebel, and J. Hamaekers, "A Molecular Dynamics Study of the Aluminosilicate Chains Structure in Al-Rich Calcium Silicate Hydrated (C-S-H) Gels," *Phys. Status Solidi (a)*, **205** [6] 1324–9 (2008).
[44]F. Puertas, M. Palacios, H. Manzano, J. S. Dolado, A. Rico, and J. Rodríguez, "A Model for the C-a-S-H Gel Formed in Alkali-Activated Slag Cements," *J. Eur. Ceram. Soc.*, **31** [12] 2043–56 (2011).
[45]I. G. Richardson and G. W. Groves, "The Structure of the Calcium Silicate Hydrate Phases Present in Hardened Pastes of White Portland Cement Blast-Furnace Slag Blends," *J. Mater. Sci.*, **32** [18] 4793–802 (1997).
[46]L. E. Malvern, *Introduction to the Mechanics of a Continuous Medium*. Prentice Hall, Englewood Cliffs, 1968.
[47]A. R. Khoei, M. J. A. Qomi, M. T. Kazemi, and A. Aghaei, "An Investigation on the Validity of Cauchy-Born Hypothesis Using Sutton-Chen Many-Body Potential," *Comput. Mater. Sci.*, **44** [3] 999–1006 (2009).
[48]A. Aghaei, M. J. A. Qomi, M. T. Kazemi, and A. R. Khoei, "Stability and Size-Dependency of Cauchy-Born Hypothesis in Three-Dimensional Applications," *Int. J. Solids Struct.*, **46** [9] 1925–36 (2009).
[49]E. B. Tadmor, M. Ortiz, and R. Phillips, "Quasicontinuum Analysis of Defects in Solids," *Philos. Mag. A-Phys. Condens. Matter Struct. Defect Mech. Prop.*, **73** [6] 1529–63 (1996).
[50]V. B. Shenoy, R. Miller, E. B. Tadmor, D. Rodney, R. Phillips, and M. Ortiz, "An Adaptive Finite Element Approach to Atomic-Scale Mechanics – the Quasicontinuum Method," *J. Mech. Phys. Solids*, **47** [3] 611–42 (1999).
[51]R. Miller, E. B. Tadmor, R. Phillips, and M. Ortiz, "Quasicontinuum Simulation of Fracture at the Atomic Scale," *Model. Simul. Mater. Sci. Eng.*, **6** [5] 607–38 (1998).
[52]V. B. Shenoy, R. Miller, E. B. Tadmor, R. Phillips, and M. Ortiz, "Quasicontinuum Models of Interfacial Structure and Deformation," *Phys. Rev. Lett.*, **80** [4] 742–5 (1998).
[53]M. J. A. Qomi, A. Aghaei, and A. R. Khoei, "Multi-Scale Modeling of Surface Effect Via the Boundary Cauchy–Born Method," *Int. J. Numer. Methods Eng.*, **85** [7] 827–46 (2011). □